Sustainable Food Proteins

WILEY

AOCS Your Global Fats and Oils Connection

ORIGINAL ARTICLE OPEN ACCESS

Effect of Cell Disruption and Protein Extraction on the Structural and Technological Properties of *Tetradesmus obliquus* Protein-Rich Extracts

César Augusto Sodré da Silva[1] | Tamires Souza Silva[1] | Nayara Flores Fonseca[1] | Rejane de Castro Santana[2] | Jose Roberto Miranda Júnior[1] | Márcio Arêdes Martins[3] | Jane Sélia dos Reis Coimbra[1]

[1]Departamento de Tecnologia de Alimentos, Universidade Federal de Viçosa, Viçosa, Brazil | [2]Departamento de Química, Universidade Federal de Viçosa, Viçosa, Brazil | [3]Departamento de Engenharia Agrícola, Universidade Federal de Viçosa, Viçosa, Brazil

Correspondence: Rejane de Castro Santana (rejane.santana@ufv.br)

Received: 30 September 2025 | **Revised:** 2 April 2026 | **Accepted:** 8 April 2026

Keywords: ball milling | DSC | emulsifying properties | FTIR | ultrasound

ABSTRACT

Microalgae, such as *Tetradesmus obliquus*, have gained attention as sustainable alternative protein sources for food. This study aimed to compare three protein extraction strategies: (P_A): ball milling followed by solubilization, (P_B): ball milling, solubilization, and isoelectric precipitation, and (P_C): ball milling combined with ultrasound, solubilization, and precipitation. We also aimed to establish the relationship between processing conditions, protein structural modifications, thermal behavior, and techno-functional properties of the resulting products. Compared to the other samples, the P_B extract exhibited the highest protein content (52.65% on a dry weight basis), although it demonstrated a lower protein recovery yield. In contrast, the P_C extract achieved the highest extraction yield, corresponding to 21.1% of the total protein in the biomass. Structurally, P_C exhibited a more ordered secondary structure, whereas P_A exhibited a less-ordered profile. Differential scanning calorimetry revealed greater thermal stability for P_C, with a denaturation enthalpy of 136.6 $J \cdot g^{-1}$, indicating stronger intermolecular interactions after ultrasound-assisted processing and precipitation, which directly influenced its functional behavior. The P_C exhibited lower water-holding capacity (0.71 ± 0.06 g water/g protein), higher oil-holding capacity (1.98 ± 0.20 g oil/g protein), and superior emulsifying performance, with creaming index values between 44.6% and 57.6% (vol/vol) and emulsifying activity index ranging from 47.2 to 89.4 m^2/g at 1% (wt/wt) concentration across pH 3.0–9.0. The main finding of this study is the clear processing–structure–function relationship established for *T. obliquus* proteins, identifying P_C strategy as the most effective method for producing protein-rich concentrates with potential applications as functional food ingredients.

1 | Introduction

Microalgae, found in almost every environment on Earth, are highly efficient organisms that have garnered interest because of their rapid growth, superior photosynthetic capabilities, and minimal carbon footprint. The biochemical composition of microalgae varies significantly based on their nutritional and cultivation conditions (Grossmann et al. 2020). Considerable research has targeted strategies to optimize biomass productivity and processes for extracting high-value substances, including lipids for biofuel production (Dias et al. 2022), proteins for food and animal feed (Grossmann et al. 2020), and carbohydrates and pigments for nutraceutical applications (Stirk et al. 2020). Developing approaches that allow the efficient recovery of various compounds is fundamental to increasing the functional and economic value of algal biomass. The key challenge lies in designing economically viable methods for achieving selective separation.

This is an open access article under the terms of the Creative Commons Attribution License, which permits use, distribution and reproduction in any medium, provided the original work is properly cited.

© 2026 The Author(s). *Sustainable Food Proteins* published by American Oil Chemists' Society and Wiley Periodicals LLC.

The green alga *Tetradesmus obliquus* exhibits rapid growth and resilience to fluctuating climate conditions. This microorganism exhibits characteristics of industrial relevance, such as a favorable fatty acid profile for advanced biofuel production and the capacity to grow in non-potable water resources, including saline and brackish environments (Vieira et al. 2021). Recent studies have demonstrated that *T. obliquus* can accumulate substantial amounts of total proteins (Amorim et al. 2020; Silva et al. 2021; Vieira et al. 2021). However, harnessing the full potential of these proteins in food applications is hindered by their encapsulation within cells protected by sturdy cell walls. The cell wall of *T. obliquus* is organized into three separate layers: an external trilaminar sheath, a fibrous middle section, and a dense inner layer adjacent to the plasma membrane (Do Carmo Cesário et al. 2022).

Various techniques have been applied to break microalgal cells for protein recovery, including mechanical disruption techniques such as bead milling, high-pressure homogenization, and ultrasonic processing (Amorim et al. 2020; Balasundaram et al. 2012; Da Silva et al. 2024; Le et al. 2025; Purdi et al. 2023; Soto-Sierra et al. 2018; Stirk et al. 2020; Ursu et al. 2014). Our preliminary investigations indicated that ultrasound is the most effective method for protein extraction from *T. obliquus* cells (Da Silva et al. 2024). Additionally, ultrasound can be readily combined with other extraction methods, such as enzymatic, mechanical, and chemical processes. These findings prompted us to investigate the potential of combining ball milling with ultrasound to improve protein extraction efficiency.

Various principles, including salting-out, isoelectric point precipitation, and solvent precipitation, can be employed to precipitate proteins released from aqueous solutions (Grossmann et al. 2020). The primary obstacle identified was maintaining the protein's native state as much as possible while ensuring that the separation process remained scalable (Grossmann et al. 2020). Alkaline solubilization, when applied before isoelectric precipitation, has been reported to enhance overall yield and quality during extraction. However, difficulties persist in scaling up these processes while preserving the desired functionality. For commercial viability, new proteins exhibit functions comparable to or enhanced (and even novel) that must function relative to existing alternatives. Recent studies (Bleakley and Hayes 2021; Grossmann et al. 2020; Taragjini et al. 2022) examining the techno-functional properties of proteins obtained from microalgae, including *Spirulina*, *Chlorella*, and various other species, highlight their promise for use in food applications. These proteins possess functional properties such as foaming, gelling, emulsification, stability, desirable sensory characteristics, and the ability to retain water or oil (known as WHC and OHC, respectively), which render them appropriate for incorporation into food formulations.

Considering these factors, this study aimed to optimize and compare protein extraction strategies from *Tetradesmus obliquus* biomass to define processing conditions that maximize protein recovery while preserving structural integrity and techno-functional performance for food applications. Three extraction approaches were evaluated: (P_A) ball milling followed by protein solubilization, (P_B) ball milling, protein solubilization, and isoelectric precipitation, and (P_C) ball milling combined with ultrasound, protein solubilization, and precipitation.

To achieve this, the protein yield and recovery were quantified, and the resulting protein concentrates were characterized in terms of their structural properties (FTIR analysis of secondary structure and differential scanning calorimetry (DSC) to assess thermal stability and denaturation behavior) and functional properties (water and oil holding capacities, emulsifying activity and stability, and macroscopic stability of emulsions). The added value of this study lies in the establishment of a direct relationship between extraction processing conditions, protein structural modifications, and techno-functional performance of the extracted protein. This approach provides scientifically grounded parameters for producing microalgal protein concentrates with enhanced functionality, thereby supporting their application as sustainable alternative protein ingredients in food systems.

2 | Materials and Methods

2.1 | Acquisition of *T. obliquus* Biomass

The *T. obliquus* BR003 strain was previously isolated from a sample of freshwater reservoirs in a Brazilian municipality, as described by Do Carmo Cesário et al. (2022). Biomass production was carried out according to previously established protocols (Da Silva et al. 2024; Vieira et al. 2021). The collected biomass was subsequently washed, freeze-dried, sieved to a standardized particle size, and stored under refrigerated (8°C ± 1°C) conditions until further use. *T. obliquus* biomass was kindly provided by the Biofuels Laboratory, Federal University of Viçosa, Brazil.

2.2 | Reagents

Sunflower oil suitable for food use (Bunge Alimentos, Brazil) was sourced from a nearby store. Deionized water, with an electrical resistivity of about 18.2 MΩ·cm at 25°C and derived from a Reference A+ purification system (Millipore, USA), was utilized in all experimental processes. The experiments utilized only analytical-grade reagents and solvents for all additional requirements.

2.3 | Protein-Rich Extract Production

Despite its considerable potential as a functional food ingredient, *T. obliquus* faces a major limitation in protein recovery due to the rigidity of its cell wall. In the microalgae industry, protein extraction typically involves two main steps: cell disruption and protein recovery (Martins et al. 2024). For that purpose, the dry biomass was initially disrupted by ball milling, and the combination of ball milling and ultrasound was also evaluated. To enhance protein extraction from *T. obliquus* biomass, the disrupted treatment was combined with physical agitation, in an alkaline medium, a technique recognized for enhancing protein solubility in this species (Silva et al. 2021). After solubilization

of the suspension, the effect of isoelectric precipitation of proteins was evaluated. The protein extraction yield (%) for each concentrate production technique was calculated using a specific equation.

$$\text{Protein Extraction Yield}\,(\%) = \frac{m_{TPC} \times p_{TPC}}{m_{TB} \times p_{TB}} \times 100\,\% \quad (1)$$

In this study, m_{TPC} represents the recovered mass (g) of the concentrated *T. obliquus* protein (TPC), p_{TPC} denotes the protein content (wt%) of TPC, m_{TB} corresponds to the initial mass (g) of *T. obliquus* biomass (TB), and p_{TB} indicates the protein content (wt%) of TB. The values of p_{TPC} and p_{TB} were determined using the Kjeldahl method, as detailed in Section 2.4.

Three different protein-rich extract production methods were evaluated:

2.3.1 | Protein Concentrated Obtained by Ball Mill Disruption and Alkaline Solubilization (P_A)

The freeze-dried biomass was mechanically pulverized using a ball mill (Tecnal Equipamentos Científicos, R-TE-350, Brazil) as described by Da Silva et al. (Da Silva et al. 2024). The sample 10 g of freeze-dried biomass was mechanically milled in a cylindrical AISI-304 stainless-steel ball mill (0.235 L). Batch processing was carried out using 0.635 cm diameter balls for 25 min at 617 rpm. The resulting powder was mixed with distilled water in a 1:10 weight-to-volume ratio (powder-to-water). The microalgal cells were homogenized (IKA RW20, Germany) for 24 h at 25°C to ensure complete rehydration. The pH of the suspension was adjusted to 10.0 and stirred (Marconi MA 502/D, Brazil) at 1500 rpm for 2 h, followed by centrifugation at 5000*g* for 5 min (Eppendorf 5430, Germany). The supernatant was collected, and the extraction process was repeated three times on the remaining biomass. The combined protein-rich supernatants were freeze-dried (Liobras L101, Brazil) to produce the concentrated protein control (P_C).

2.3.2 | Protein Concentrated Obtained by Ball Mill Disruption and Isoelectric Precipitation (P_B)

To precipitate proteins extracted after ball mill rupture of biomass and solubilization at pH 10.0, the soluble proteins achieved in the supernatant underwent partial adjustment to pH 2.5, which corresponds to the isoelectric point (Silva et al. 2021). After adjusting the pH using 1 mol/L HCl, the mixtures were subjected to centrifugation at 5000× g for 10 min. The precipitate obtained was then collected, frozen at −20°C, and subsequently freeze-dried (Liobras, L101, Brazil) to yield protein-concentrated P_B.

2.3.3 | Protein Concentrated Obtained by Ball Mill and Ultrasound Disruption Techniques and Isoelectric Precipitation (P_C)

In this section, protein extraction was tested using a combination of cell disruption methods. The biomass previously disrupted by ball milling was resuspended in distilled water at a concentration of 10.0% (wt/vol) and subjected to magnetic stirring for 24 h. Subsequently, the suspensions were further disrupted using a tip sonicator (Sonics, VCX 500, USA) under the conditions established by Silva et al. (Da Silva et al. 2024), at a frequency of 20 kHz and 98% amplitude for 6 min of ultrasonication. The cells were disrupted by cooling in an ice bath to avoid overheating the system. Following the disruption, the microalgal suspension's pH was set to 10.0, then it underwent magnetic stirring and centrifugation. The resulting supernatant, containing dissolved proteins, was collected. This extraction process was conducted three times in succession. The protein-rich supernatants were then adjusted to pH 2.5, the isoelectric point, to precipitate the proteins. The obtained precipitate was stored at −20°C and later freeze-dried (Liobras, L101, Brazil) to yield the protein-enriched P_C.

2.4 | Proximate Composition of the *T. obliquus* Biomass and Protein Concentrates

The dried *T. obliquus* biomass, P_A, P_B, and P_C extracts underwent proximate composition analysis. This included measuring moisture (AOAC 2005); ash (AOAC 2005); lipids, and proteins. Lipid quantification in *T. obliquus* biomass was performed using the Folch method (Folch et al. 1957). For protein extracts, the gravimetric difference after Soxhlet extraction with petroleum ether as the solvent was employed (AOAC 2005). Protein determination was performed via the Kjeldahl method (AOAC 2005), using a nitrogen-to-protein conversion factor of 5.89 (Afify et al. 2018), which is based on the amino acid profile of this species. Afify et al. (Afify et al. 2018) reported that ~10% of the total nitrogen in *T. obliquus* originates from non-protein nitrogen (NPN) compounds, such as pigments, nucleic acids, glucosamine, and amines; this contribution was considered in the selection of the conversion factor used in this study. Carbohydrates were calculated by difference, based on 100% less the contributions of moisture, ash, lipids, and proteins.

The pigments from protein-rich extracts were extracted and measured according to method adapted from Wellburn (1994), with adjustments to use an 80% acetone solution in the extraction process. Pigments were extracted by adding pure acetone (30 mL per 100 mg of sample) and incubating them in sealed tubes for 12 h at room temperature in the dark. The extracts were centrifuged (Eppendorf 5430, Germany) at 7100 × g for 10 min, and the supernatant was filtered through quantitative filter paper (C40, Unifil, Brazil). Pigment concentrations were determined spectrophotometrically (Shimadzu UV-1800, Japan) using empirical Equations (2–4). All measurements were performed in triplicate.

$$Ca = 12.25 \times A_{663.2} - 2.79 \times A_{646.8} \quad (2)$$

$$Cb = 21.50 \times A_{646.8} - 5.10 \times A_{663.2} \quad (3)$$

$$Cc = 1000 \times A_{470} - 1.82 \times Ca - 85.02 \times Cb\,/\,198 \quad (4)$$

In this context, C_a, C_b, and C_c indicate the concentrations of chlorophyll a (μg/mL), chlorophyll b (μg/mL), and total carotenoids (μg/mL), respectively, with A representing the absorbance of the pigments at specific wavelengths. After extraction and quantification, the results were expressed as a percentage

(% [mg pigment/100 mg microalgae]) by relating the total extract volume to the mass of the biomass used, as described below:

$$\%\,(\mathrm{mg}/100\,\mathrm{mg}) = 100 \times \frac{C \times V \times 10^{-3}}{m} \quad (5)$$

Here, C represents the concentration of chlorophyll a, chlorophyll b, or total carotenoids (μg/mL); V denotes the total volume of the extract (mL); and m corresponds to the mass of the protein extract (mg)

The color properties of the protein extracts were evaluated using a CR-10 colorimeter (Konica Minolta, Japan). Measurements were performed in the CIELab color space, yielding the parameters lightness (L*), redness (a), and yellowness (b).

2.5 | Structural Characterization of Protein-Rich Extracts From *T. obliquus*

2.5.1 | FTIR Spectroscopy

Protein-rich extracts from *T. obliquus* were subjected to FTIR spectroscopy using a 660-IR spectrophotometer (Varian) with a GladiATR attenuated reflectance accessory (PIKE Technologies). The analysis covered a wavenumber range of 400–4000 cm^{-1}, employing 16 scans at a spectral resolution of 4 cm^{-1}. This method was used to evaluate the functional groups present in the *T. obliquus* protein-rich extract powders by measuring their transmittance across a specified range. The secondary structural elements of the protein-rich extracts were identified using the amide I band (1700–1600 cm^{-1}) by calculating the ratio of the area of each component's peak to the total area of the structures.

2.5.2 | Differential Scanning Calorimetry

Protein-rich extracts from *T. obliquus* were examined using a Q1000 differential scanning calorimeter (DSC) from TA Instruments, based in New Castle, DE, USA. For this analysis, a 5 mg sample was combined with 15 μL of water and left to hydrate for 24 h before testing. The samples were then placed in aluminum pans for DSC analysis. The temperature gradually increased from 20°C to 400°C at a rate of 10°C/min. The resulting thermograms were evaluated using Universal Analysis 2010 software (TA Instruments) to determine the peak denaturation temperature (Td) and enthalpy of denaturation (ΔHd).

2.6 | Techno-Functional Properties of Protein Concentrates

2.6.1 | Water and Oil Holding Capacities (WHC and OHC, Respectively)

The capacities for holding water and oil were evaluated using a modified version of the method outlined by Omura et al. (2021). A 0.1 g sample of protein-rich *T. obliquus* extract was placed in microtubes and combined with 1 g of either Milli-Q water or sunflower oil. The procedure included vortexing (Phoenix, Recnal, Brazil) for 10 s every 5 min over a 30-min period, followed by centrifugation at 10,000*g* for 15 min. After removing the supernatant, the tubes containing the pellets were weighed. This allowed the measurement of the amount of water or oil retained by the protein isolate. WHC and OHC were expressed as grams of absorbed water or oil per gram of protein extract and calculated using Equation (6):

$$WHC\ or\ OHC\,(\%) = \frac{W_2 - W_1}{W_0} \times 100\,\% \quad (6)$$

In Equation (6), W_1 represents the weight of the centrifuge tube with the dry sample, W_2 corresponds to the weight of the tube after removal of oil or water, and W_0 denotes the initial sample weight.

2.6.2 | Emulsifying Properties

2.6.2.1 | Preparations of the Emulsions. Microalgal protein emulsions were formulated in 50 mL Falcon-type tubes. The emulsion ingredients consisted of: (1) sunflower oil; (2) 0.03% (wt/vol) sodium azide to inhibit microbial growth; and (3) an aqueous protein concentrate solution with concentrations of 1.0%, 2.0%, and 4.0% (wt/vol), adjusted to pH levels of 3.0, 5.0, 7.0, and 9.0 using 1 M hydrochloric acid or sodium hydroxide solutions. Overnight agitation of the continuous phases was performed at 25.0°C ± 1.0°C, ensuring pH regulation through monitoring and adjustment. The emulsions consisted of 75% (wt/wt) protein extract dispersed in water (continuous phase) and 25% (wt/wt) sunflower oil (dispersed phase) in the continuous phase. Emulsification was performed using an Ultra-Turrax device (T25, IKA-Werke GmbH & Co., Germany) at 10,000 rpm for 5 min. Each emulsion was prepared in triplicate.

2.6.2.2 | Emulsifying Activity Index (EAI). The EAI of the emulsions was evaluated by using a modified version of the method described by Oliveira et al. (De Oliveira et al. 2020). In summary, 50 μL aliquots were taken from 2 cm below the surface of freshly prepared emulsions and diluted 1:200 in 0.1% sodium dodecyl sulfate (SDS). The sample absorbance at 500 nm was measured using a UV–vis spectrophotometer (Cary 50, Varian, Australia) with a 1 cm path-length plastic cuvette. The EAI was subsequently calculated according to the following equation:

$$EAI\left(\frac{m^2}{g}\right) = \frac{2 \times 2{,}303 \times A_0 \times DF}{C \times \emptyset \times 10000} \quad (7)$$

In Equation (7), A_0 corresponds to the absorbance of the freshly prepared diluted emulsion. DF indicates the dilution factor (×200), C represents the protein concentration in the aqueous phase prior to emulsion formation, and ϕ denotes the oil fraction of the emulsion (0.25).

2.6.2.3 | Microstructure. After a week of storage under kinetic equilibrium conditions, the emulsions were scrutinized using a Zeiss Primo Star iLED optical microscope. The samples were placed on slides with coverslips and observed under a microscope at a magnification of 40×. For each sample, a minimum of 10 images were captured and analyzed using

TABLE 1 | Proximate composition (%) of *T. obliquus* biomass and protein concentrate.

	T. obliquus biomass	P_A	P_B	P_C
Moisture % (wt/wt)	7.87 ± 0.10	15.69 ± 0.07[a]	8.19 ± 0.04[c]	5.34 ± 0.21[b]
Ash % (wt/wt)	18.33 ± 0.03	33.62 ± 1.02[a]	8.60 ± 0.61[b]	8,34 ± 0.11[b]
Total Lipids % (wt/wt)	4.23 ± 0.22	1.38 ± 0.21[c]	4.37 ± 0.64[b]	14.07 ± 0.16[a]
Proteins % (wt/wt)	40.29 ± 0.24	26.58 ± 0.39[c]	48.34 ± 0.61[a]	43.55 ± 0.87[b]
Carbohydrates **% (wt/wt)	29.28	22.73	30.60	28.36
Protein Yield (%)		8.93 ± 0.46[b]	3.77 ± 0.19[c]	21.10 ± 0.32[a]
Chlorophyll a % (wt/wt)		ND	0.01 ± 0.00	0.24 ± 0.01
Chlorophyll b % (wt/wt)		ND	0.01 ± 0.01	0.05 ± 0.01
Carotenoids% % (wt/wt)		0.17 ± 0.02	0.60 ± 0.07	3.10 ± 0.24
L*		68.28 ± 0.08	41.39 ± 0.01	37.71 ± 0.01
A		−0.48 ± 0.01	1.60 ± 0.01	0.30 ± 0.02
B		19.45 ± 0.03	5.42 ± 0.03	1.85 ± 0.02
Appearance				

Note: P_A: Protein concentrate from BM disruption (lyophilized supernatant). P_B: Protein concentrate from BM disruption with isoelectric precipitation; P_C: Protein concentrate from BM and ultrasound disruption with isoelectric precipitation. L* denotes lightness and ranges from 0 (black) to 100 (white), with a (+) red, a (−) green, b (+) yellow, and b (−) blue. **No standard deviation data, as the difference calculation obtained carbohydrate content. Means with different letters differ by Tukey's test ($p < 0.05$).
Abbreviation: ND, not detected.

ImageJ 1.50i (http://rsb.info.nih.gov/ij/). The diameters of at least 500 droplets per sample were measured and are displayed as frequency histograms. The surface mean diameter (d_{32}) was determined using Equation (8), where d_i represents the droplet diameter, and n_i denotes the number of droplets of that specific diameter.

$$d_{32} = \frac{\sum n_i d_i^3}{\sum n_i d_i^2} \quad (8)$$

2.6.2.4 | **Macroscopic Stability of Emulsions.** The macroscopic kinetic stability of the emulsions was assessed using the Creaminess Index (CI). Freshly prepared emulsions (10 mL) were transferred to 15 mL Falcon tubes and stored vertically at room temperature. The lower serum height (H_s) and total emulsion height (H_t) were recorded over a seven-day period, and images were captured according to the same schedule. CI was calculated using Equation (9).

$$CI\,(\%) = \frac{H_S}{H_t} \times 100\% \quad (9)$$

2.7 | Statistical Analysis

All experiments were performed in triplicate, and the data are presented as mean ± standard deviation. Statistical differences among treatments were evaluated using one-way ANOVA followed by Tukey's test (at a 5% significance level) and *t*-tests.

3 | Results and Discussion

3.1 | Proximate Composition of *T. obliquus* Biomass and Protein Concentrate

Table 1 summarizes the centesimal composition of *T. obliquus* biomass and protein concentrate. The composition of this microalga varies with growth conditions, influencing the accumulation of the desired components (Rocha et al. 2019). *T. obliquus* biomass is rich in proteins, lipids, and carbohydrates, which are highly valued in the food industry. Before disruption, the algal biomass contained a protein content of 43.73% (dry weight basis), which is consistent with previous reports describing *T. obliquus* biomass as having a high protein content (Amorim et al. 2020; Do Carmo Cesário et al. 2022; Rocha et al. 2019; Scoculi De Lira et al. 2025; Silva et al. 2021; Vieira et al. 2021). The biomass exhibits a protein concentration that exceeds the levels typically reported in conventional animal protein sources, including beef (22%), chicken (24%), fish (24%), and skimmed milk (36%) (Bleakley and Hayes 2021). Additionally, proteins confined within cells and organelles may not exhibit their full functional potential in vivo. An effective approach to improve the digestibility of algal proteins involves disrupting the cell wall, thereby enabling the solvent to reach intracellular proteins (Soto-Sierra et al. 2018).

This study evaluated a combination of techniques to promote protein release by diffusion through membranes and walls. Given that the experiment utilized dry biomass, the disruption

process was initiated using ball milling. Ball milling is known for its cost-effectiveness, allowing large volumes of biomass to be processed in batches and enabling gravity-based separation of the disrupted biomass (Balasundaram et al. 2012). It has also been proven to be effective in breaking *T. obliquus* cells (Amorim et al. 2020; Vieira et al. 2021). After breaking down the biomass, it was hydrated and stirred under alkaline conditions. A pH of 10 was chosen based on the study by Silva et al. (Silva et al. 2021), who found that the dissolution of *T. obliquus* biomass at a pH of nearly 10.0 can promote protein extraction due to its maximal solubility at this value. After solubilization, the suspension was centrifuged, and the supernatant containing the dissolved proteins was freeze-dried (P_A extract) or precipitated using the isoelectric point (pI) (P_B extract).

As can be seen in Table 1, the protein concentrate produced by BM disruption and freeze-drying of the supernatant (P_A) had the lowest protein content at 31.53% on a dry weight basis. Although the protein content from isoelectric precipitation (P_B and P_C) was significant, further disruption using ultrasound (P_C) produced a greater protein yield than the other methods tested. However, the extract contained a significant amount of ash content. The substantial mineral content in microalgal biomass is due to the absorption of large quantities of minerals from the environment. This process is essential for DNA synthesis, maintaining osmotic balance, and supporting enzymatic activity, among other functions (Rocha et al. 2019). Although the mineral fraction may impose certain limitations on the utilization of biomass and protein concentrates, the biomass ash content was below 10.15% ± 0.03% reported by Lima et al. (2023), who utilized a freeze-dried crude biomass supernatant to produce a protein extract.

According to the data obtained, the extract produced through precipitation (P_B extract) had a higher protein content (52.65% on a dry weight basis) than the other extracts, despite having a lower protein recovery yield. The acid precipitation method was chosen because of its simplicity, low cost, and advantages over methods such as salts or ethanol, which may complicate downstream processing or introduce unwanted compounds into the precipitate (Martins et al. 2024). However, the low efficiency of protein recovery using acid precipitation is not surprising, as only solubilized proteins can be precipitated. In mechanical rupture, intracellular components are released along with proteins through the compromised cell wall. Protein solubility is enhanced by selecting an alkaline medium; however, under these conditions, hydroxide ions permeate the algal cell wall and membrane, react with intracellular lipids, resulting in the saponification of triglycerides into glycerol and fatty acid anions (Le et al. 2025). These non-protein elements precipitate with proteins in an acidic environment.

To increase protein recovery from biomass, a combination of ball milling and ultrasound, a method of cell disruption, was evaluated. Ultrasonication generates high shear forces and cavitation, producing substantial mechanical stress on the cell wall, which facilitates the release of intracellular constituents, including proteins (Le et al. 2025). This combined approach disrupts the integrity of the cell wall and membrane in microalgal cells (Soto-Sierra et al. 2018). These openings enhance the permeability of the cell wall, facilitating solvent penetration and promoting protein release (Rida et al. 2024). Additionally, cavitation may induce protein unfolding, thereby improving their capacity to establish covalent interactions with other molecules, such as polysaccharides (Le et al. 2025). As a result, non-protein constituents, including carbohydrates and pigments, were released alongside the proteins. Thus, although the P_C extract presented the highest protein concentration among the other extracts produced, it was still not possible to achieve a high level of protein purity in this extract (46.01% on a dry weight basis).

The methodology applied for protein extraction also resulted in the simultaneous release of pigments, as can be seen in the pigment values and color parameters presented in Table 1. *T. obliquus* is a photosynthetic microalga that is rich in chlorophyll and carotenoids. Carotenoids are pigments with provitamin A activity and antioxidant properties that have generated considerable interest in the food industry because of the increasing demand for naturally colored and nutritionally enriched foods (Uenojo et al. 2007). As shown in Table 1, the color characteristics of the protein extracts provided important insights into their pigment composition, particularly regarding chlorophylls and carotenoids. In the present study, the colorimetric parameters (L*, a*, and b*) obtained from the three protein extracts were analyzed concerning the concentrations of chlorophyll a, chlorophyll b, and total carotenoids.

P_A extract exhibited no detectable chlorophyll a or b, while containing a low concentration of carotenoids. The P_A extract presented a light color with a strong yellow hue (*b*+) and a very slight greenish hue (*a*−). Its color profile was characterized by a high lightness, slightly negative a* value, and markedly high b* value. The elevated b* value reflects the dominance of yellow pigments, whereas the high L* value suggests a low pigment density or high purity of the extract. These parameters indicated a bright yellowish tone, consistent with the presence of isolated carotenoids and the absence of chlorophyll interference.

The P_B extract presented a darker coloration than the P_A, with slight red and moderate yellow components, producing a light brown coloration. P_B extract showed low levels of both chlorophyll a and b (0.01% each), along with a mild concentration of carotenoids. This sample exhibited lower lightness, a positive a* value, and a reduced b* value. The increased a* value and lower b* may indicate the beginning of pigment oxidation or the presence of degradation products, possibly resulting in a brown hue. The slight increase in the red-green balance and decrease in yellow intensity imply partial masking of carotenoids by residual chlorophylls.

The P_C protein-rich extract showed significant quantities of pigments. This significant amount of pigments can also be verified in the coloration of the darkest sample, which exhibited almost neutral tones and a very faint yellow hue, likely resulting from the co-localization of pigments and the overlapping of chlorophyll and carotenoid absorption spectra. It showed the lowest lightness, a nearly neutral a* value, and a very low b* value. The absence of yellow dominance (low b*) despite the high carotenoid concentration indicates a strong masking effect by chlorophylls, which dominate the visual appearance of the extract.

3.2 | Structural Characterization of the Protein Concentrate of the Microalga *T. obliquus*

In general, chemical bonds exhibit characteristic stretching and bending vibrations at distinct energy levels, generating specific absorption bands in the infrared region. The analysis of the position, width, and intensity of these bands enables the identification of the molecular composition and functional groups.

Figure 1 shows the infrared absorption spectra of three protein extract samples across the range of 4000–400 cm^{-1}. The FTIR analysis demonstrated consistent absorption patterns across all samples, with peaks at the same wavenumbers, indicating similar chemical compositions. However, differences in peak intensities suggest variations in the relative amounts or concentrations of the components among the samples. In analyzing carbohydrate structures, five characteristic spectral regions can be identified within the mid-infrared range (4000–400 cm^{-1}), as described by Ordóñez et al. (Gómez-Ordóñez and Rupérez 2011): (i) the O—H and C—H stretching region (3600–2800 cm^{-1}); (ii) the region related to local symmetry (1500–1200 cm^{-1}); (iii) the C—O stretching region (1200–950 cm^{-1}); (iv) the fingerprint or anomeric region (950–700 cm^{-1}); and (v) the skeletal vibration region below 700 cm^{-1}. As shown in Figure 1, the spectra of the cellular biomass from the analyzed green algae display a broad absorption band in the 3000–3600 cm^{-1} range, with a peak around 3290 cm^{-1} (Piasecka et al. 2020). This band is characteristic of O—H stretching vibrations related to water, as well as N—H stretching vibrations from protein functional groups (Piasecka et al. 2020) and polysaccharides such as starch and cell wall carbohydrates (Srimongkol et al. 2023). The band at 2899 cm^{-1} corresponds to C—H stretching vibrations of aliphatic groups, commonly associated with carbohydrate backbones. The signal at 2347 cm^{-1} is due to atmospheric CO_2 and is not directly related to biomass composition. The region between 1200 and 900 cm^{-1}, where carbohydrates exhibit strong absorption, is marked by the prominent band at 1049 cm^{-1}. This band can be assigned to C—O and C—O—C stretching vibrations of glycosidic linkages, indicating the presence of glucose-based polysaccharides, especially starch (Do Carmo Cesário et al. 2022). Additionally, the band at 1228 cm^{-1} might be due to S═O stretching vibrations, implying the presence of sulfate groups and supporting the existence of sulfated extracellular polysaccharides (EPS), as previously reported for this species (Yu et al. 2024). The band at 1426 cm^{-1} is associated with CH_2 bending vibrations, which is also consistent with carbohydrate structures. Lastly, the low-frequency band near 616 cm^{-1} may be related to sulfate vibrations or polysaccharide skeletal modes, further supporting the possible presence of sulfated carbohydrates (Yu et al. 2024).

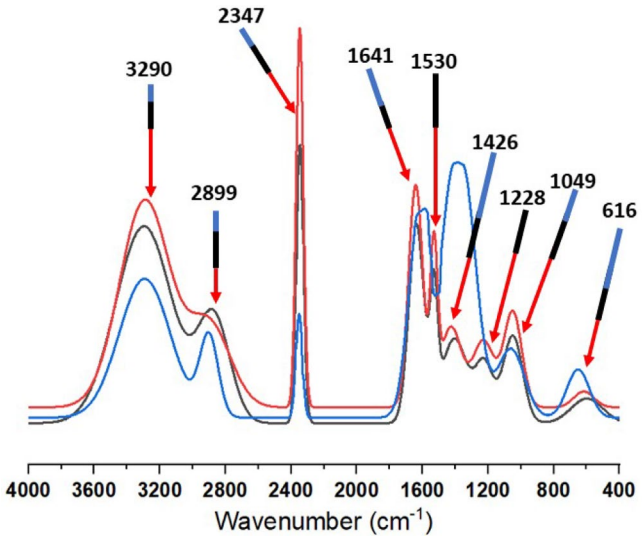


FIGURE 1 | Infrared (FTIR) spectrum in the range of 4000 to 400 cm^{-1} for the three protein extract samples produced: Protein concentrate produced by disrupting BM and freeze-drying the supernatant—P_A (blue), protein concentrate from BM disruption with isoelectric precipitation—P_B (black), protein concentrate from BM and ultrasound disruption with isoelectric precipitation P_C (red).

In practice, the FTIR spectra of proteins are recorded in the amide I region because this band (mainly arising from the C═O stretching of the peptide bond) is highly sensitive to the protein secondary structure. Each resolved band is then assigned to a structural motif (α-helix, β-sheet, β-turn, or random coil), allowing a semi-quantitative estimation of the protein conformational composition. Figures 2–4 show the FTIR spectra of the protein-rich extracts in the amide I region (1700–1600 cm^{-1}), where the upper curves represent the fitted profiles with the generated peaks (P1–P8), and the lower curves indicate the hidden components (A1–A8) obtained from second-derivative analysis and Gaussian deconvolution.

The amide I band, which mainly arises from the C═O stretching vibrations of peptide bonds, is highly sensitive to the protein secondary structure; therefore, the deconvoluted components were assigned to the following characteristic motifs: β-turns at 1692–1661 cm^{-1} (except 1678–1672 cm^{-1}), α-helices at 1660–1650 cm^{-1}, random coils at 1649–1641 cm^{-1}, β-sheets at 1640–1610 cm^{-1} (with an additional component at 1678–1672 cm^{-1}), and aggregates near 1618 cm^{-1} (Cai and Singh 2004; Secundo and Guerrieri 2005; Timilsena et al. 2016). The findings indicated that the FTIR spectra of the three protein-rich extracts (P_A, P_B, and P_C) exhibited variations, particularly in the absorption intensity of certain characteristic peaks.

The relative amount of each component of the protein secondary structure (Table 2) was calculated as a percentage of the area under the (hidden) peaks in the original spectra, attributed to specific secondary structures. Secondary structure analysis of the amide I band revealed distinct profiles among the three samples; thus, it can be inferred that the structures of these proteins are not similar, which may provide different physicochemical and functional properties. Analysis of the secondary structure revealed that β-sheet is the predominant secondary structure in these protein extracts. Overall, increased β-sheet content corresponded to reduced flexibility, whereas α-helix variations contributed to structural diversity across the samples.

The P_A protein-rich extract exhibited a balanced composition with moderate β-sheet (43.00 ± 2.25) and α-helix (18.68 ± 1.04) content, higher β-turn (20.69 ± 5.32) and random coil (13.66 ± 2.11) content, and a small fraction of aggregates (3.96 ± 0.08), indicating a mixture of ordered and flexible regions, however, a higher proportion of β-turns and random coils implies a lower stability of the protein. The P_B protein-rich extract exhibited an intermediate β-sheet content (51.69 ± 0.92) in

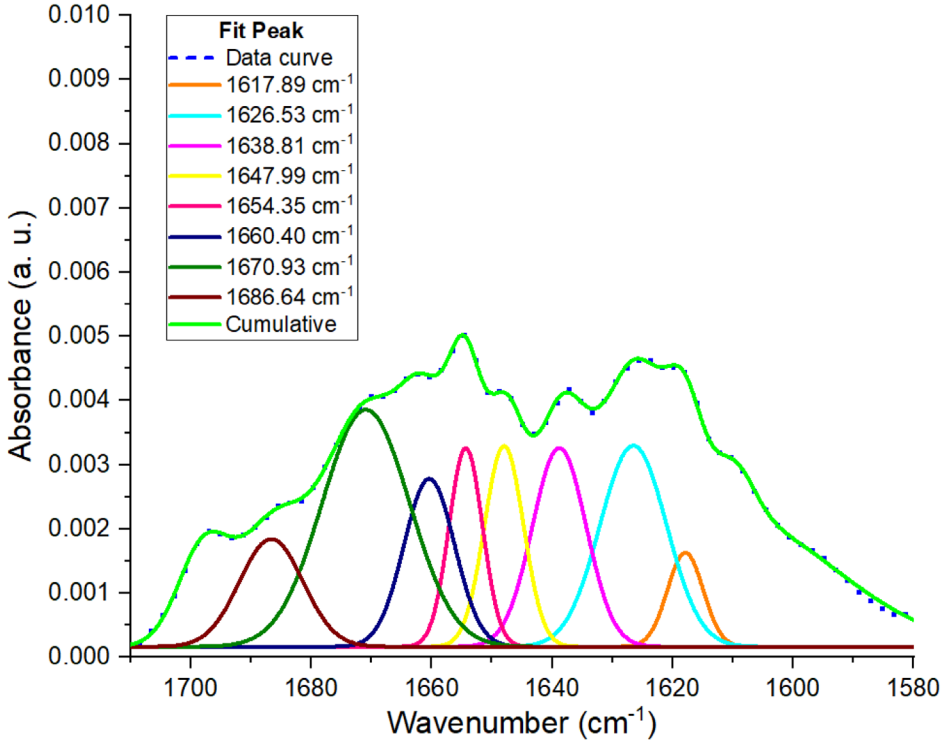


FIGURE 2 | Infrared (FTIR) spectrum in the region of the amide I band (1600–1700 cm^{-1}) of the protein concentrate produced by disrupting BM and freeze-drying the supernatant (P_A). The coefficient of determination of the fit was $R^2 = 0.99906$.

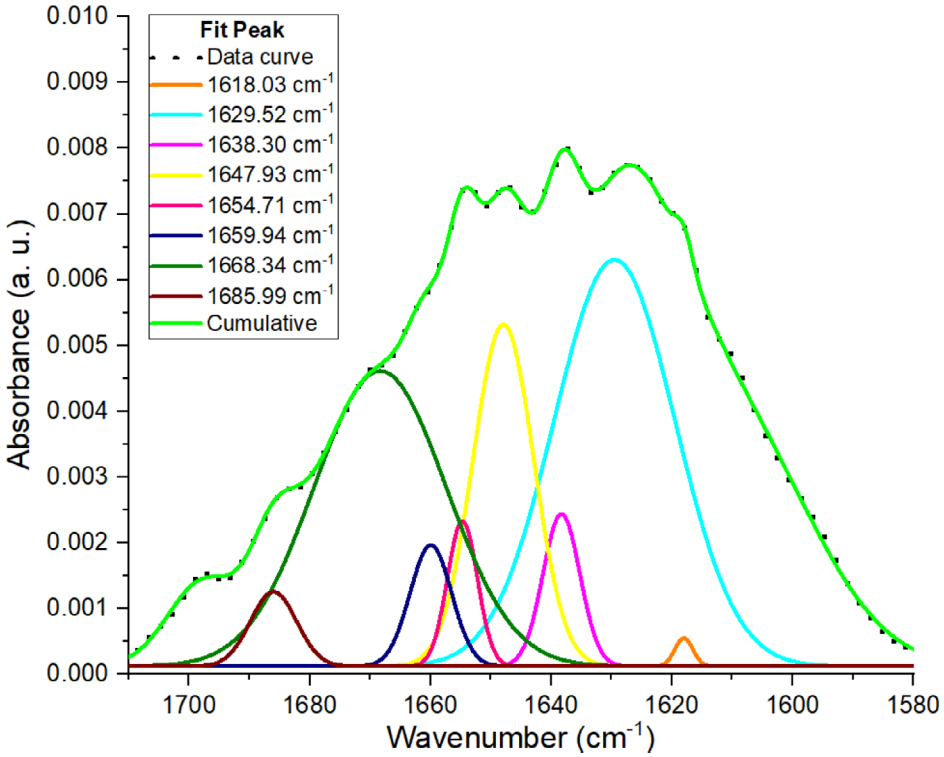


FIGURE 3 | Infrared (FTIR) spectrum in the region of the amide I band (1600–1700 cm^{-1}) of the protein concentrate from BM disruption with isoelectric precipitation (P_B). The coefficient of determination of the fit was $R^2 = 0.99878$.

combination with the highest α-helix proportion (27.41 ± 0.62), moderate β-turns (15.42 ± 2.26), low random coil content (5.17 ± 0.69), and minimal aggregate formation (0.31 ± 0.02), indicating a stable structure with some flexibility. The P_C protein-rich extract was highly β-sheet-rich (73.26 ± 5.98) with minimal β-turns (7.02 ± 3.47), random coils (3.07 ± 0.11), and

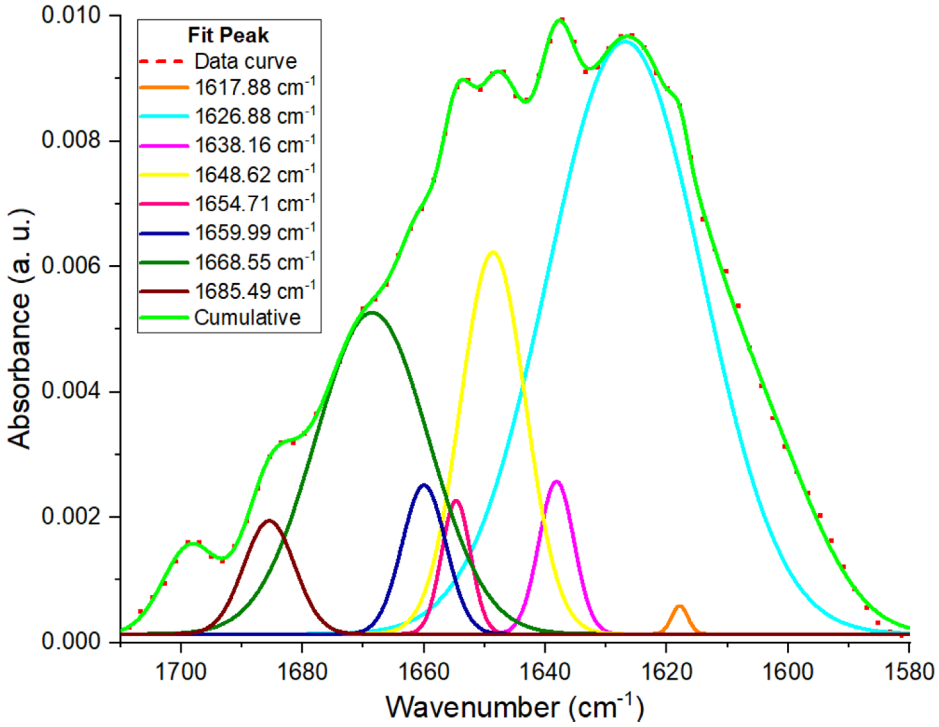


FIGURE 4 | Infrared (FTIR) spectrum in the region of the amide I band (1600–1700 cm^{-1}) of the protein concentrate from BM and ultrasound disruption with isoelectric precipitation (P_C). The coefficient determination of the fit was $R^2 = 0.99647$.

TABLE 2 | Attributions of secondary structures of amide band I components in protein-rich extracts. The secondary composition of the amide I band components is presented as the means ± standard deviations ($n = 3$).

Secondary structure components	Band location range (cm^{-1})	Proportion of each component in the amide I band (%)		
		P_A	P_B	P_C
β-turns	1692–1661 (except 1678–1672)	20.69 ± 5.32[a]	15.42 ± 2.26[a]	7.02 ± 3.47[b]
α-helix	1660–1650	18.68 ± 1.04[b]	27.41 ± 0.62[a]	16.40 ± 2.40[b]
Random coils	1649–1641	13.66 ± 2.11[a]	5.17 ± 0.69[b]	3.07 ± 0.11[c]
β-sheet	1640–1610 (except 1618) 1678–1672	43.00 ± 2.25[c]	51.69 ± 0.92[b]	73.26 ± 5.98[a]
Aggregate structures	1618	3.96 ± 0.08[a]	0.31 ± 0.02[b]	0.26 ± 0.00[c]

Note: The results are presented as mean ± standard deviation ($n = 3$). Identical letters in the same column indicate no significant statistical differences ($p < 0.05$). P_A: Protein concentrate from BM disruption (lyophilized supernatant). P_B: Protein concentrate from BM disruption with isoelectric precipitation. P_C: Protein concentrates from BM and ultrasound disruption with isoelectric precipitation. Means with different letters differ by Tukey's test ($p < 0.05$).

low aggregates (0.26 ± 0.00), reflecting a more ordered and rigid protein structure. This implies that the P_C protein-rich extract is the most structurally stable and has greater potential for interaction with other molecules owing to its more linear configuration.

Although the P_A and P_B extracts originated from the same protein source, their structural profiles differed markedly because of the processing route. The P_B extract was produced by isoelectric precipitation, a process that involves pH adjustment to the protein isoelectric point, leading to charge neutralization, reduced solubility, and enhanced protein–protein interactions (PPI). These conditions favor aggregation and conformational rearrangements, resulting in changes in the secondary structure, as detected by FTIR analysis, compared to the P_A extract.

Similar behavior has been reported for both model and food proteins, where aggregated proteins exhibit a higher β-sheet content than their native forms. Nagano et al. (2023) investigated the mechanism of pH-responsive precipitation of cell surface protein B, a major extracellular secretion protein of *Corynebacterium glutamicum*. The authors demonstrated that protein precipitation triggered by pH changes near the isoelectric point was accompanied by a transition toward β-sheet-rich structures, detectable by ATR-FTIR (notably at ~1624 cm^{-1}), indicating that conformational rearrangement plays a key role in aggregation and precipitation of proteins.

Similarly, Gkinali et al. (2022) reported that FTIR analysis of proteins recovered from defatted *Tenebrio molitor* larvae by alkaline extraction followed by isoelectric precipitation yielded a

protein fraction dominated by β-structures, comprising 37.59% β-sheet and 34.20% β-turn structures, whereas random coils were the least prevalent conformation (8.79%). These findings are consistent with the results obtained in the present study for the P_B extract.

Studies on co-precipitated plant proteins have also employed FTIR spectroscopy to assess the secondary structure differences between pH-driven assemblies and simple protein blends, further demonstrating the influence of pH adjustment and precipitation on protein folding patterns (L. Wang et al. 2025). According to these authors, co-precipitation induces synergistic folding and intimate protein–protein interactions, promoting peptide chain rearrangement and ultimately resulting in co-precipitated proteins with more compact and structured secondary conformations.

In relation to the other samples, the P_C extract was produced using a combination of cell disruption caused by ultrasound and ball milling. As shown in Table 2, ultrasound treatment led to significant changes in the secondary structures of the P_C extract. Compared to the P_B extract, the β-sheet content increased, whereas the α-helix and β-turn content decreased ($p < 0.05$). Several studies have used FTIR spectroscopy to assess the impact of ultrasound on protein structure, which might be attributed to the disruption of hydrogen bonds within peptide molecules. For example, sonication of soy protein hydrolysates produced significant changes in the secondary structure, including increased β-sheet and decreased α-helix content, indicating ultrasound-induced unfolding and aggregate disruption (Tian et al. 2020). Wen et al. (2019) revealed that sonication promoted a shift in the secondary structure of watermelon seed protein, with β-sheet and α-helix contents increasing from 33.52% to 38.57% and decreasing from 11.81% to 6.03%, respectively.

Similar behavior was observed in studies that worked with different types of protein sources, such as sonication of mushroom polyphenol oxidase (Baltacıoğlu et al. 2017) and myofibrillar proteins from *Tenebrio molitor* (X. Wang et al. 2024) and soy protein isolate (Zhao et al. 2019), consistent with ultrasound-induced unfolding and exposure of hydrophobic groups. FTIR analysis of coconut protein after ultrasound treatment documented changes in the secondary structure that correlated with improved functional properties, illustrating how ultrasound can modify protein conformation in food systems (Sun et al. 2022). The lack of random coil conformation endows the P_C protein-rich extract with a more defined and rigid structure, potentially enhancing its thermal stability and solubility in aqueous environments, as well as improving the texture, gel, and foam formation of the protein, or reducing the protein flexibility and water-holding capacity (WHC).

The thermal denaturation temperature (Td) and enthalpy of formation (ΔH) are key parameters for describing the thermal behavior of a sample, which reflect its stability and structural order. The ΔH value reflects the number of bonds required to maintain a protein's folded structure and is determined by the area under the endothermic peak; a higher ΔH indicates greater energy, suggesting that more energy is required for protein unfolding. ΔH represents the proportion of undenatured protein in a sample and is correlated with the extent of the ordered structure of a protein (Tang and Sun 2011). The thermal denaturation of proteins is influenced by several factors, including the extraction method, pre-treatment procedures, heating, and solvent use (Waghmare et al. 2016). The thermal stability of the protein fractions in the extracts was evaluated using differential scanning calorimetry (DSC). The temperature associated with protein denaturation is called the melting point of the material (Td), which corresponds approximately to the maximum melting peak on the thermogravimetric curve. In general, the protein extracts showed high thermal resistance to denaturation: P_A presented 135.40°C, with an associated enthalpy of 46.86 $J \cdot g^{-1}$; P_B presented 121.87°C, with an associated enthalpy of 51.12 $J \cdot g^{-1}$; and P_C presented 114.20°C, with an associated enthalpy of 136.60 $J \cdot g^{-1}$.

The differences observed among P_A, P_B, and P_C can be explained by the distinct disruption and extraction processes applied. In P_A treatment, mechanical disruption promoted protein release but may also have induced partial unfolding due to shear forces, resulting in proteins that remained relatively soluble and less aggregated. Consequently, P_A exhibited the highest Td and lowest ΔH, requiring less energy to break the bonds. This is consistent with its secondary structure, which has the lowest β-sheet content and the highest random coil and aggregate contents (Table 2). It requires less energy (low ΔH) because it has a less ordered structure. However, the remaining structures were more heat-stable; thus, the transition only occurred at higher temperatures (higher Td), making P_A a suitable candidate for foods subjected to thermal processing. In P_B, the additional isoelectric precipitation step reduced the electrostatic repulsion near the protein isoelectric point, promoting aggregation through hydrophobic interactions and structural rearrangement. This typically leads to more compact protein assemblies and, therefore, to increased Td values. In contrast, the high acidity used for protein precipitation of P_B and P_C maintains the α-helix or β-sheet content (high ΔH) but weakens their thermal stability (low Td). In P_C, ultrasound-induced cavitation can transiently expose hydrophobic regions and enhance protein–protein interactions without significantly increasing the bulk temperature, favoring the formation of stronger aggregated networks after precipitation. The P_C extract presented the highest ΔH value (136.6 $J \cdot g^{-1}$), and this discrepancy may arise due to the greater proportion of β-sheets observed in its FTIR analysis, which positively influences (Shevkani et al. 2015).

Another point worth noting is the carbohydrate concentration in P_B and P_C extracts. Agustinisari et al. (2024) suggested that protein-carbohydrate conjugation tends to increase ΔH, reflecting the greater energy required to denature the protein, which is interpreted as greater thermal stability of the complex. Kusumastuti et al. (2024) evaluated the thermal properties of Spirulina (*Arthrospira platensis*) protein concentrate after its interaction with carrageenan via conjugation (Maillard reaction). The authors verified that the observed increase in thermal stability could be due to the polysaccharide's ability to influence protein folding, thereby affecting the three-dimensional structure and enhancing overall stability. These findings underscore the necessity of selecting pretreatments not solely based on extraction yield but also on compound stability, particularly in applications where thermosensitivity and formulation integrity are essential, such as in functional food or pharmaceutical product development.

3.3 | Techno-Functional Properties of Protein Concentrates

Cell disruption is a key step in microalgal protein processing because the rigid structure of the cell wall requires considerable energy to break, directly affecting the process costs. In addition, the adopted disruption method can impact downstream purification efficiency and influence the structural and techno-functional properties of the final protein ingredient (Nunes et al. 2024). As shown in Table 1, the protein extraction yields from *T. obliquus* biomass were lower when only ball milling was applied. In contrast, the sequential experimental strategy combining ultrasound and agitation promoted more effective cell rupture, increasing the availability of intracellular components and consequently, protein recovery. An advantage of ultrasound treatment is the high extraction yield of valuable compounds (De Oliveira et al. 2020; Sun et al. 2022; Tian et al. 2020; X. Wang et al. 2024; Wen et al. 2019; Zhao et al. 2019). Although more intense disruption enhances protein release from the microalgal matrix, ultrasound requires a cooling system to avoid temperatures above 35°C, as it provokes protein denaturation, reducing extraction yields and bio-functionality (Nunes et al. 2024). Therefore, an appropriate balance between disruption efficiency and protein structural preservation is essential to optimize both the yield and techno-functional quality.

The protein content of the extracts ranged from 31.53% to 52.65% on a dry weight basis. This finding suggests that non-protein substances have distinct characteristics, as they were not effectively eliminated. Hydrophilic components enhance WHC, whereas hydrophobic amino acids increase the OHC (López et al. 2019). The water-holding capacities (WHC) of the three extracts are shown in Figure 5. WHC is defined as the protein's potential to retain its intrinsic water and any additional water under applied stress, and this characteristic is directly linked to the texture and sensory perception of foods (Hong et al. 2024; Nunes et al. 2024).

The P_B extract exhibited the highest WHC (2.73 ± 0.07 g water/g protein) compared to the other extracts. The enhanced WHC of the P_B extract is likely associated with multiple structural and compositional attributes, including reduced protein solubility, higher phosphate group content, smaller particle and pore dimensions, specific pH conditions, and decreased proportion of α-helical structures, all of which contribute to improved protein hydration (Chen et al. 2019). Bleakley and Hayes (2021) isolated proteins from *Spirulina* sp. and *Isochrysis galbana* T-Iso, reporting WHC values of 2.25 g water/g protein extract and 0.47 g water/g protein extract, respectively. Chen et al. (2019) found the following WHC values for protein extracts produced by *Chlorella pyrenoidosa* (2.02 g water/g protein), *Arthospira platensis* (2.81 g water/g protein), and *Nannochloropsis oceanica* (2.87 ± 0.07 g water/g protein). Hong et al. (2024) reported that among four microalgae species, *Euglena gracilis* displayed the highest WHC (2.87 g water/g protein), followed by *Chlamydomonas reinhardtii* (1.88 g water/g protein), *Spirulina platensis* (1.69 g water/g protein), and *Spirulina maxima* (1.58 g water/g protein). This study also indicated that the amino acid profile of the protein is a key factor influencing WHC. As can be seen, these values are comparable to those obtained for the extracts produced in our study.

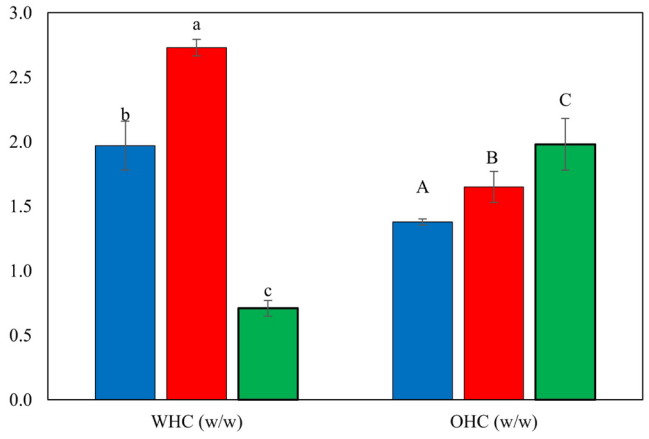


FIGURE 5 | Water holding capacity (WHC) and oil holding capacity (OHC) of P_A (■), P_B (■), and P_C (■). Lowercase letters compare the WHC means, whereas capital letters compare the OHC means. Different letters differ by Tukey's test ($p < 0.05$).

The oil holding capacity (OHC) is a fundamental property in protein functionality studies, serving as an indicator of the binding potential of hydrophobic groups to lipid phases. An increased ability to interact with lipids is closely associated with the EAI and sensory qualities, such as improved mouthfeel, better palatability, and flavor retention, making it suitable for high-fat foods (Bleakley and Hayes 2021; Nahimana et al. 2024). The OHC of the three extracts is presented in Figure 5. The highest OHC was observed in the P_C extract (1.98 ± 0.20 g oil/g protein), followed by the P_B (1.65 ± 0.12 g oil/g protein) and P_A (1.38 ± 0.02 g oil/g protein) extracts. The high OHC value found in the P_C extract can be explained by the effect of ultrasound on cell disruption. As noted by Omura et al. (2021), ultrasound induced an increase in surface hydrophobicity in nearly all systems, indicating partial protein unfolding or denaturation and greater exposure of hydrophobic groups, which can interact favorably with triglyceride molecules. Although the OHC of these three extracts was lower than that reported in other studies for some microalgae, such as *Spirulina* (5.80 g water/g protein), *Isochrysis* sp.(3.16 g water/g protein), *Arthospira platensis* (8.37 ± 1.45 g oil/g protein), *Nannochloropsis oceanica* (8.25 ± 0.44 g oil/g protein), and *Chlorella pyrenoidosa* (6.68 ± 0.41 g oil/g protein) (Bleakley and Hayes 2021; Chen et al. 2019).

The ability of the three extracts to act as emulsifiers, an essential functional trait of proteins, was evaluated across different pH levels using the creaming index (CI) and EAI. The EAI measures the effectiveness of a protein as an emulsifier, which involves the stabilization of a mixture of two immiscible liquids, such as oil and water. The CI reflects the physical instability of the emulsion, with a stable emulsion ideally showing little to no phase separation and thus having a low CI. The emulsifying properties of the emulsions were notably affected by both pH and protein concentration. Moreover, variations in the type and amount of proteins present in the extracts, along with the tendency of these molecules to aggregate, may influence their emulsifying properties (Chen et al. 2019). The kinetic stabilities of the emulsions are shown in Figure 6. Generally, phase separation occurred faster in emulsions prepared with P_A extract or at low pH and slower in emulsions with P_A extract or under alkaline conditions. Moreover, increasing the extract concentration decreased the volume and velocity of phase separation, especially in emulsions with P_B and P_C concentrates.

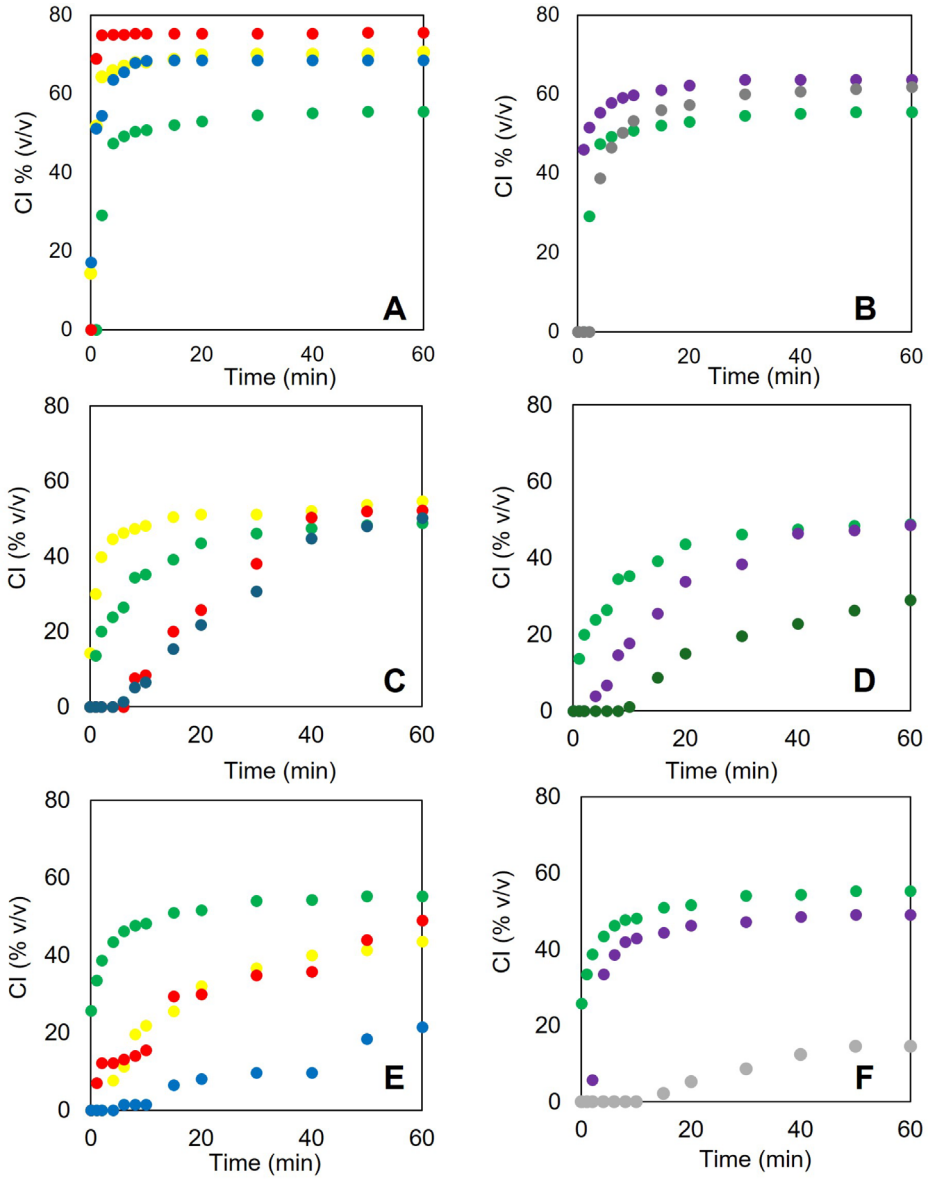


FIGURE 6 | Creaming index (CI) over 60 min of emulsions with 1% (wt/wt) of protein extract at pH 3 (●), 5 (●), 7 (●), and 9 (●), and emulsions with 1% (●), 2% (●), and 4% (●) (wt/wt) of protein extract at pH 5.0. Extraction types: P_A (A and B), P_B (C and D), and P_C (E and F).

The EAI and CI after 7 days of storage are presented in Figure 8. As anticipated, the EAI and CI exhibited different behaviors in each extract. The emulsions produced with P_B and P_C extracts were more stable than those produced with the P_A extract, which can be attributed to the lowest OHC (Figure 5). This behavior can be attributed to the composition of the P_A extract, which had the highest ash content among all evaluated samples. When salt is present at high concentrations (salting-out effect), water molecules in the medium preferentially interact with the dissociated ions rather than with the protein molecules, as the solvation of smaller particles (ions) is energetically favored. Consequently, water initially associated with proteins is displaced, enhancing protein–protein interactions and reducing their solubility in the aqueous phase, ultimately leading to precipitation (Costa et al. 2025). This process causes a loss of kinetic stability and results in the separation of the emulsion into its original phase. This behavior was even more pronounced when emulsions produced with different P_A extract concentrations were compared (Figure 7B), and greater instability was observed as the protein concentration increased. For the P_A extract, the highest EAI was observed at pH 5.0, whereas the other pH values were lower. At a pH of 5.0, the P_A extract had values like those of the other extracts. In addition, unlike the others produced under acidic conditions, the P_A extract was obtained by freeze-drying an extract prepared at a basic pH.

The high stability observed in the P_B extract can be attributed to the concentration and presence of sufficient proteins in the emulsion that can adequately cover the oil droplets and form a stable interfacial film. Moreover, the presence of non-protein elements in protein isolates from algae and cyanobacteria may influence their emulsifying ability (Teuling et al. 2019). For instance, it has been demonstrated that charged carbohydrates, which may naturally be present in algal protein extracts, can contribute to the stabilization of emulsions, preventing flocculation (Schwenzfeier et al. 2014).

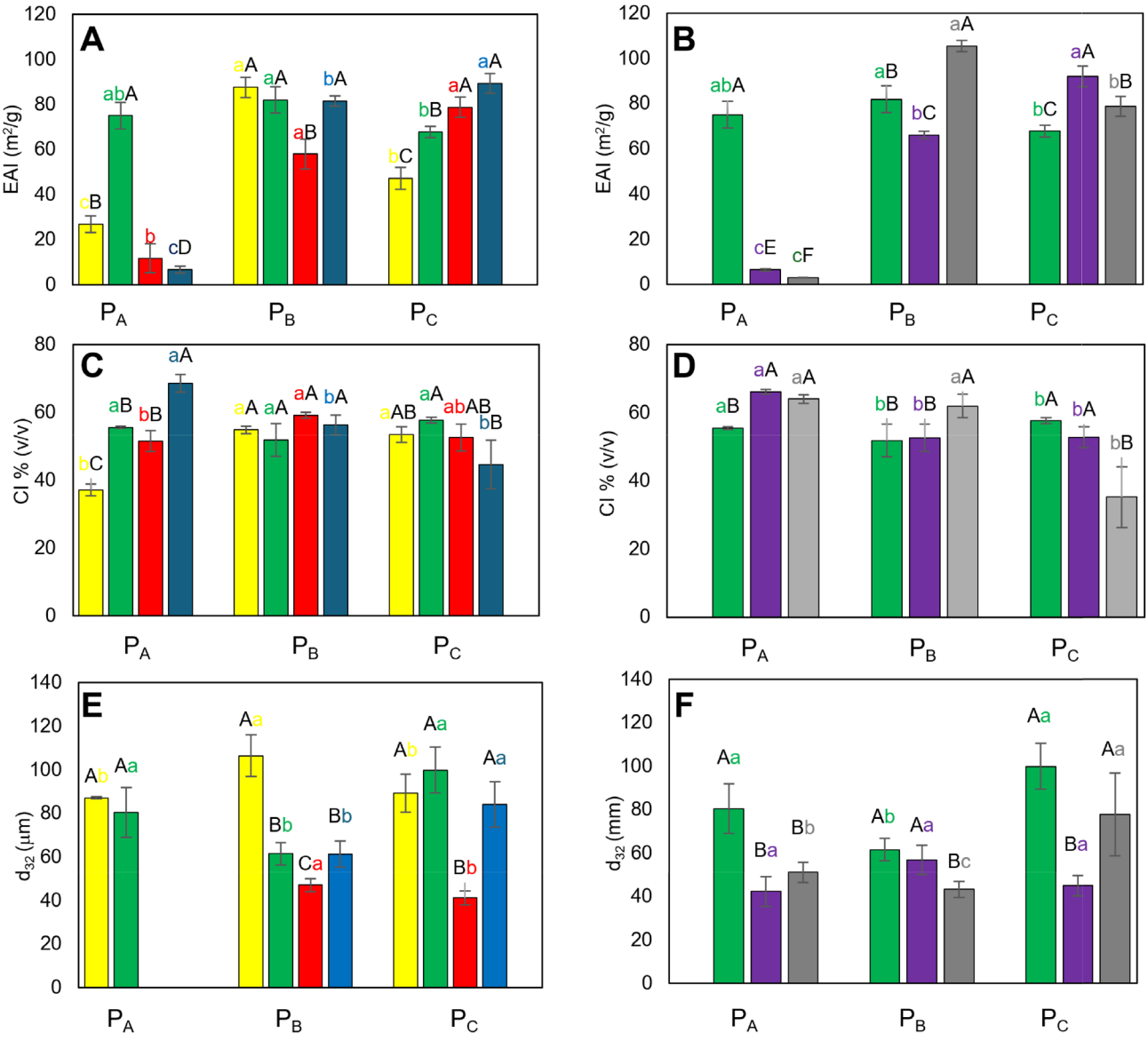


FIGURE 7 | EAI (emulsifying activity index, m^2/g), CI (creaming index, % vol/vol), and d_{32} (mean droplet size, mm) of emulsions with 1% (wt/wt) extract at pH 3 (■), 5 (■), 7 (■), and 9 (■), and emulsions with 1 (■), 2 (■), and 4 (■) % (wt/wt) extract at pH 5.0. Colored lowercase letters compare the means between protein extracts (P_A, P_B, and P_C) (at the same pH or concentration). Black capital letters indicate comparisons of means of the same extract at different pH or concentration levels.

In summary, P_C extract was the most effective protein for occupying the oil–water interface, as it significantly reduced surface tension and maintained emulsion stability by preventing the coalescence of oil droplets. The EAI and CI of the P_C extract exhibited a pH-dependent pattern, consistent with the findings of Chen et al. (2019) regarding various protein extracts from three microalgae species: *Chlamydomonas reinhardtii*, *Euglena gracilis*, *Spirulina platensis*, and *Spirulina maxima*. They linked this behavior to differences in solubility between the two solvents. As depicted in Figure 7A, the P_C extracts reached their lowest EAI values at pH 3.0, close to their pI, while achieving peak values at pH 9.0. Protein solubility is heavily affected by pH. The decreased EAI at acidic pH is likely due to protein precipitation at the isoelectric point, where reduced solubility and loss of charge decrease electrostatic repulsion, leading to droplet destabilization (Grossmann et al. 2020). Surface charge also plays a critical role. Near the pI, the reduction in net charge promotes intermolecular aggregation and precipitation, thereby constraining the structural rearrangements and limiting interfacial unfolding. Under these conditions, solubility is minimized, which restricts the capacity of proteins to adsorb at the oil–water interface. In contrast, higher solubility favors emulsification, as it facilitates the rapid migration of protein molecules to droplet surfaces, where they assemble into a cohesive viscoelastic interfacial network that stabilizes the emulsion by limiting droplet flocculation and coalescence (Hong et al. 2024). As indicated by the OHC results, the P_C extract exhibited greater hydrophobicity, which contributed to its emulsification ability.

The effect of pH on the emulsifying properties depends on the protein extract type. The emulsions containing 1% P_B extract at pH 3.0–9.0 showed similar CI (between 51.9% and 59.1% [vol/

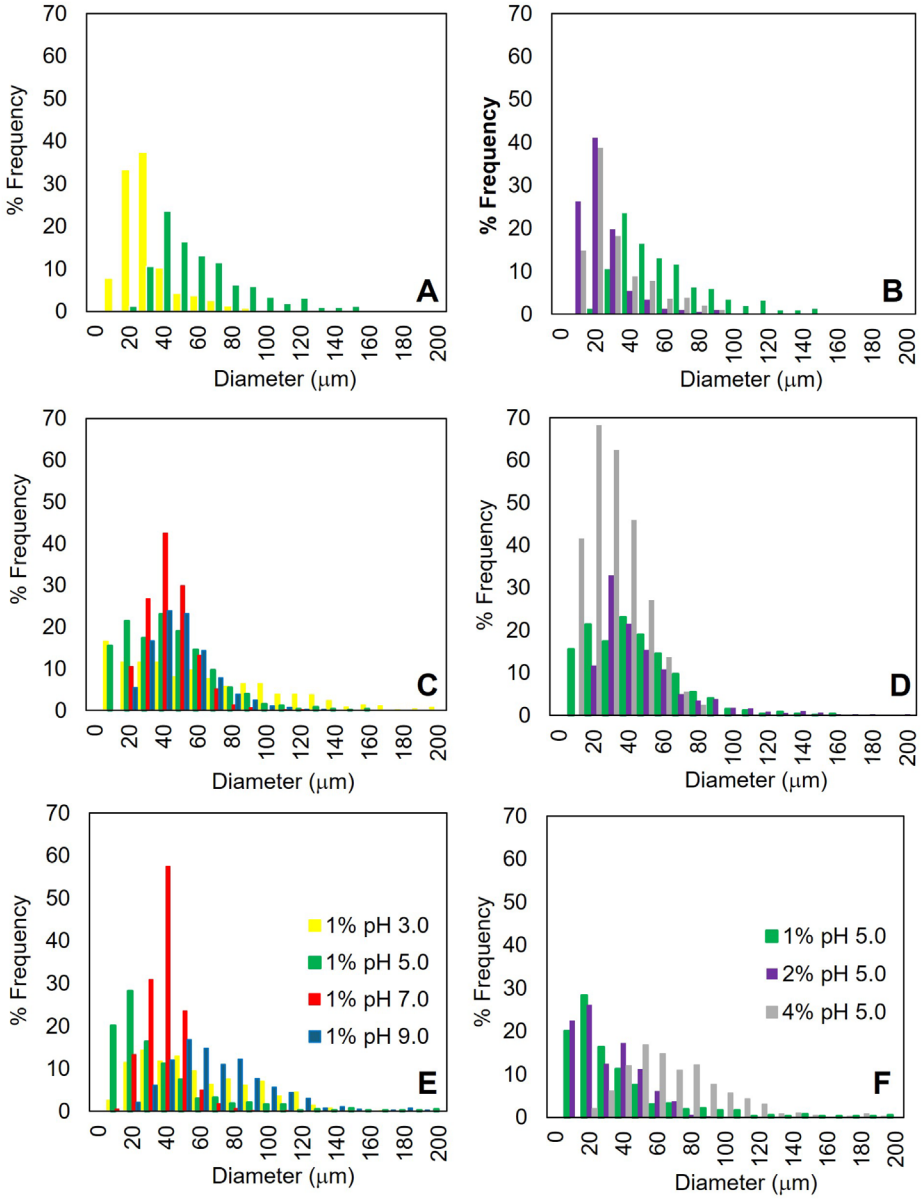


FIGURE 8 | Droplet size distribution of emulsions with 1% (wt/wt) extract at pH 3 (●), 5 (●), 7 (●), and 9 (●), and emulsions with 1% (●), 2% (●), and 4% (●) (wt/wt) extract at pH 5.0. Extract types: P_A extract (A and B), P_B extract (C and D), and P_C extract (E and F).

vol]) (Figure 7C) with the lowest EAI (57.99 m^2/g) at pH 7.0. The emulsions containing 1% P_C extract concentrate at pH 3.0–9.0 showed a CI between 44.6% and 57.6% (vol/vol) and EAI between 47.2 and 89.4 m^2/g. EAI increased with pH, while CI decreased with pH, resulting in an emulsion at pH 9.0 with the highest EAI (89.39 m^2/g) and the lowest CI (44.58% vol/vol). In contrast, the pH increase led to a decrease in EAI and a slight increase in CI in emulsions with P_B extract.

The mean droplet size (d_{32}) and droplet size distribution of the emulsions are shown in Figures 7 and 8, respectively. Except for the systems with P_A extract at pH 7.0 and 9.0, the emulsions exhibited a microstructure with droplets surrounded by a continuous aqueous phase. Generally, d_{32} decreased with increasing protein content (Figure 7F), whereas the effect of pH on emulsion droplet size was unclear (Figure 7E). Emulsions with P_A extract showed similar d_{32} values at pH 3.0 and 5.0, whereas systems at pH 7.0 and 9.0 did not show oil droplets. The P_B extract emulsion showed a decrease in d_{32} with an increase in pH from 3.0 to 5.0, remaining constant at higher pH values. The emulsions with P_C extract concentrate exhibited similar d_{32} values at pH 3.0, 5.0, and 9.0, and a lower d_{32} at pH 7.0.

4 | Conclusions

The current study provides further insights into protein recovery following various extraction techniques. Among the methods tested, the combination of extraction techniques effectively disrupted the microalgal cell wall, releasing intracellular proteins while preserving their natural structures. Moreover, the use of isoelectric precipitation to isolate proteins helps lower operational costs, as the precipitate can be readily dried. This approach resulted in high-quality protein extracts that are suitable for comprehensive proteome analysis and potentially for other applications. Among the extracts produced, the P_C extract

showed 43.55% protein content, which presented a stable secondary structure (73.26% β-sheet structure and 16.40% α-helix) and denaturation enthalpy of 136.6 J·g^{-1}. These characteristics resulted in the highest OHC, lowest WHC, and best ability to stabilize emulsions among the protein-rich extracts. Moreover, considering its high pigment concentration, it may function as a carrier system for hydrophobic bioactive compounds in emulsion formulations.

Author Contributions

César Augusto Sodré da Silva designed the conceptualization, developed the methodology, carried out the formal analysis, investigation, analyzed the data, provided resources, supervision, data curation, and prepared the original draft of the manuscript. Tamires Souza Silva, Nayara Flores Fonseca, and Jose Roberto Miranda Júnior carried out research experiments, reviewed, and edited the manuscript. Rejane de Castro Santana reviewed the methodology, supervised the experimental work, reviewed, edited the manuscript, and provided resources. Márcio Aredes Martins and Jane Sélia dos Reis Coimbra reviewed, edited the manuscript, acquired funding, and provided resources. All authors have read and agreed to the published version of the manuscript.

Acknowledgments

This research received financial support from various Brazilian entities, such as the Fundação de Amparo à Pesquisa do Estado de Minas Gerais (Fapemig, APQ-02267-22), the Conselho Nacional de Desenvolvimento Científico e Tecnológico (CNPq), the Financiadora de Estudos e Projetos (Finep), and the Coordenação de Aperfeiçoamento de Pessoal de Nível Superior—Brazil (CAPES)—Finance Code 001. In addition, Petroleo Brasileiro S.A. (Petrobras) also funded the project.

Funding

This work was supported by the Fundação de Amparo à Pesquisa do Estado de Minas Gerais (Fapemig, APQ-02267-22), the Conselho Nacional de Desenvolvimento Científico e Tecnológico (CNPq), the Financiadora de Estudos e Projetos (Finep), and the Coordenação de Aperfeiçoamento de Pessoal de Nível Superior—Brazil (CAPES)—Finance Code 001. In addition, Petroleo Brasileiro S.A. (Petrobras) also funded the project.

Ethics Statement

The authors have nothing to report.

Conflicts of Interest

The authors declare no conflicts of interest.

References

Afify, A. E.-M. M. R., G. S. El Baroty, F. K. El Baz, H. H. Abd El Baky, and S. A. Murad. 2018. "*Scenedesmus obliquus*: Antioxidant and Antiviral Activity of Proteins Hydrolyzed by Three Enzymes." *Journal of Genetic Engineering and Biotechnology* 16, no. 2: 399–408. https://doi.org/10.1016/j.jgeb.2018.01.002.

Agustinisari, I., K. Mulia, N. Harimurti, et al. 2024. "The Potency of Maillard Conjugates Containing Whey Protein as Natural Emulsifier." *International Journal of Food Science* 2024: 1–21. https://doi.org/10.1155/2024/3254132.

Amorim, M. L., J. Soares, B. B. Vieira, W. Batista-Silva, and M. A. Martins. 2020. "Extraction of Proteins From the Microalga *Scenedesmus obliquus* BR003 Followed by Lipid Extraction of the Wet Deproteinized Biomass Using Hexane and Ethyl Acetate." *Bioresource Technology* 307: 123190. https://doi.org/10.1016/j.biortech.2020.123190.

AOAC. 2005. *Official Methods of Analysis*. AOAC.

Balasundaram, B., S. C. Skill, and C. A. Llewellyn. 2012. "A Low Energy Process for the Recovery of Bioproducts From Cyanobacteria Using a Ball Mill." *Biochemical Engineering Journal* 69: 48–56. https://doi.org/10.1016/j.bej.2012.08.010.

Baltacıoğlu, H., A. Bayındırlı, and F. Severcan. 2017. "Secondary Structure and Conformational Change of Mushroom Polyphenol Oxidase During Thermosonication Treatment by Using FTIR Spectroscopy." *Food Chemistry* 214: 507–514. https://doi.org/10.1016/j.foodchem.2016.07.021.

Bleakley, S., and M. Hayes. 2021. "Functional and Bioactive Properties of Protein Extracts Generated From Spirulina Platensis and *Isochrysis galbana* T-Iso." *Applied Sciences* 11, no. 9: 3964. https://doi.org/10.3390/app11093964.

Cai, S., and B. R. Singh. 2004. "A Distinct Utility of the Amide III Infrared Band for Secondary Structure Estimation of Aqueous Protein Solutions Using Partial Least Squares Methods." *Biochemistry* 43, no. 9: 2541–2549. https://doi.org/10.1021/bi030149y.

Chen, Y., J. Chen, C. Chang, et al. 2019. "Physicochemical and Functional Properties of Proteins Extracted From Three Microalgal Species." *Food Hydrocolloids* 96: 510–517. https://doi.org/10.1016/j.foodhyd.2019.05.025.

Costa, J. E. G., J. D. S. Matos, P. Z. Azevedo, et al. 2025. "Techno-Functionality of Jack Bean (*Canavalia ensiformis*) Protein Concentrate: A Comparative Study With Soy and Pea Proteins." *Journal of the Science of Food and Agriculture* 105, no. 6: 3439–3452. https://doi.org/10.1002/jsfa.14108.

Da Silva, C. A. S., K. V. M. Sibaja, S. De Ramos Cizilio, et al. 2024. "Evaluation of Cell Rupture Techniques for the Extraction of Proteins From the Microalgae Tetradesmus Obliquus." *Phycology* 4, no. 1: 87–103. https://doi.org/10.3390/phycology4010005.

De Oliveira, A. P. H., M. H. Omura, É. D. A. A. Barbosa, et al. 2020. "Combined Adjustment of pH and Ultrasound Treatments Modify Techno-Functionalities of Pea Protein Concentrates." *Colloids and Surfaces A: Physicochemical and Engineering Aspects* 603: 125156. https://doi.org/10.1016/j.colsurfa.2020.125156.

Dias, C., B. P. Nobre, J. A. L. Santos, T. Lopes Da Silva, and A. Reis. 2022. "Direct Lipid and Carotenoid Extraction From *Rhodosporidium toruloides* Broth Culture After High Pressure Homogenization Cell Disruption: Strategies, Methodologies, and Yields." *Biochemical Engineering Journal* 189: 108712. https://doi.org/10.1016/j.bej.2022.108712.

Do Carmo Cesário, C., J. Soares, J. F. S. Cossolin, et al. 2022. "Biochemical and Morphological Characterization of Freshwater Microalga Tetradesmus Obliquus (Chlorophyta: Chlorophyceae)." *Protoplasma* 259, no. 4: 937–948. https://doi.org/10.1007/s00709-021-01712-3.

Folch, J., M. Lees, and G. H. Sloane Stanley. 1957. "A Simple Method for the Isolation and Purification of Total Lipides From Animal Tissues." *Journal of Biological Chemistry* 226, no. 1: 497–509.

Gkinali, A.-A., A. Matsakidou, and A. Paraskevopoulou. 2022. "Characterization of *Tenebrio molitor* Larvae Protein Preparations Obtained by Different Extraction Approaches." *Food* 11, no. 23: 3852. https://doi.org/10.3390/foods11233852.

Gómez-Ordóñez, E., and P. Rupérez. 2011. "FTIR-ATR Spectroscopy as a Tool for Polysaccharide Identification in Edible Brown and Red Seaweeds." *Food Hydrocolloids* 25, no. 6: 1514–1520. https://doi.org/10.1016/j.foodhyd.2011.02.009.

Grossmann, L., J. Hinrichs, and J. Weiss. 2020. "Cultivation and Downstream Processing of Microalgae and Cyanobacteria to Generate Protein-Based Technofunctional Food Ingredients." *Critical Reviews*

in Food Science and Nutrition 60, no. 17: 2961–2989. https://doi.org/10.1080/10408398.2019.1672137.

Hong, X., L. Fan, X. Yan, and J. Li. 2024. "Structural and Functional Properties of Proteins Isolated From Four Species of Microalgae and Their Application in Air-Water Interface Stabilization." *International Journal of Biological Macromolecules* 283: 137531. https://doi.org/10.1016/j.ijbiomac.2024.137531.

Kusumastuti, M. R., S. Yuliani, C. Hidayat, and A. D. Setiowati. 2024. "Modification Techno-Functional Properties of Spirulina Protein Concentrates (*Arthrospira platensis*) as O/W Emulsifier by Conjugation and Electrostatic Complexations." *Innovative Food Science & Emerging Technologies* 95: 103727. https://doi.org/10.1016/j.ifset.2024.103727.

Le, T. P. L., J. Samarathunga, M. Gabard, K. Strazdins, J. Rens, and B. Adhikari. 2025. "Comparison of Extraction Methods to Obtain High-Purity Protein Concentrate From Green Microalgae *Nannochloropsis oceanica*." *Sustainable Food Technology* 3, no. 2: 549–558. https://doi.org/10.1039/D4FB00387J.

Lima, V. S., D. R. B. De Oliveira, C. A. S. Da Silva, et al. 2023. "Stabilization of Oil–Water Emulsions With Protein Concentrates From the Microalga Tetradesmus Obliquus." *Journal of Food Science and Technology* 60, no. 2: 797–808. https://doi.org/10.1007/s13197-023-05666-7.

López, D. N., M. Galante, G. Raimundo, D. Spelzini, and V. Boeris. 2019. "Functional Properties of Amaranth, Quinoa and Chia Proteins and the Biological Activities of Their Hydrolyzates." *Food Research International* 116: 419–429. https://doi.org/10.1016/j.foodres.2018.08.056.

Martins, P. L., L. C. Duarte, H. Pereira, A. Reis, and F. Carvalheiro. 2024. "Evaluation of Different Fractionation Methods for the Simultaneous Protein and Carbohydrate Extraction From Microalgae." *Biomass Conversion and Biorefinery* 15: 999–1011. https://doi.org/10.1007/s13399-024-05279-w.

Nagano, H., T. Mannen, Y. Kikuchi, and K. Shiraki. 2023. "The pH-Responsive Precipitation–Redissolution of the CspB Fusion Protein, CspB50TEV-Teriparatide, Triggered by Changes in Secondary Structure." *Biochemistry and Biophysics Reports* 33: 101435. https://doi.org/10.1016/j.bbrep.2023.101435.

Nahimana, P., I. Bouaicha, C. Chèné, et al. 2024. "Physico-Chemical, Functional, and Structural Properties of Un-Defatted, Cold and Hot Defatted Yellow Lupin Protein Isolates." *Food Chemistry* 437: 137871. https://doi.org/10.1016/j.foodchem.2023.137871.

Nunes, E., K. Odenthal, N. Nunes, T. Fernandes, I. A. Fernandes, and M. A. A. Pinheiro De Carvalho. 2024. "Protein Extracts From Microalgae and Cyanobacteria Biomass. Techno-Functional Properties and Bioactivity: A Review." *Algal Research* 82: 103638. https://doi.org/10.1016/j.algal.2024.103638.

Omura, M. H., A. P. H. De Oliveira, L. D. S. Soares, et al. 2021. "Effects of Protein Concentration During Ultrasonic Processing on Physicochemical Properties and Techno-Functionality of Plant Food Proteins." *Food Hydrocolloids* 113: 106457. https://doi.org/10.1016/j.foodhyd.2020.106457.

Piasecka, A., A. Nawrocka, D. Wiącek, and I. Krzemińska. 2020. "Agro-Industrial By-Product in Photoheterotrophic and Mixotrophic Culture of Tetradesmus Obliquus: Production of ω3 and ω6 Essential Fatty Acids With Biotechnological Importance." *Scientific Reports* 10, no. 1: 6411. https://doi.org/10.1038/s41598-020-63184-4.

Purdi, T. S., A. D. Setiowati, and A. Ningrum. 2023. "Ultrasound-Assisted Extraction of Spirulina Platensis Protein: Physicochemical Characteristic and Techno-Functional Properties." *Journal of Food Measurement and Characterization* 17, no. 5: 5474–5486. https://doi.org/10.1007/s11694-023-02051-y.

Rida, H., J. Peydecastaing, H. Takache, A. Ismail, and P.-Y. Pontalier. 2024. "Comparison of Tetraselmis Suecica Cell Disruption Techniques: Kinetic Study and Extraction of Hydrosoluble Compounds." *Processes* 12, no. 6: 1139. https://doi.org/10.3390/pr12061139.

Rocha, D. N., M. A. Martins, J. Soares, et al. 2019. "Combination of Trace Elements and Salt Stress in Different Cultivation Modes Improves the Lipid Productivity of Scenedesmus spp." *Bioresource Technology* 289: 121644. https://doi.org/10.1016/j.biortech.2019.121644.

Schwenzfeier, A., P. A. Wierenga, M. H. M. Eppink, and H. Gruppen. 2014. "Effect of Charged Polysaccharides on the Techno-Functional Properties of Fractions Obtained From Algae Soluble Protein Isolate." *Food Hydrocolloids* 35: 9–18. https://doi.org/10.1016/j.foodhyd.2013.07.019.

Scoculi De Lira, G., I. A. Severo, F. A. Ferraz, et al. 2025. "Multiparametric Evaluation of Tetradesmus Obliquus Biomass: An Integrated Approach Including Antioxidant, Nutritional, and Energy Properties." *Microorganisms* 13, no. 7: 1583. https://doi.org/10.3390/microorganisms13071583.

Secundo, F., and N. Guerrieri. 2005. "ATR-FT/IR Study on the Interactions Between Gliadins and Dextrin and Their Effects on Protein Secondary Structure." *Journal of Agricultural and Food Chemistry* 53, no. 5: 1757–1764. https://doi.org/10.1021/jf049061x.

Shevkani, K., N. Singh, A. Kaur, and J. C. Rana. 2015. "Structural and Functional Characterization of Kidney Bean and Field Pea Protein Isolates: A Comparative Study." *Food Hydrocolloids* 43: 679–689. https://doi.org/10.1016/j.foodhyd.2014.07.024.

Silva, M. E. T. D., M. A. Leal, M. D. O. Resende, M. A. Martins, and J. S. D. R. Coimbra. 2021. "*Scenedesmus obliquus* Protein Concentrate: A Sustainable Alternative Emulsifier for the Food Industry." *Algal Research* 59: 102468. https://doi.org/10.1016/j.algal.2021.102468.

Soto-Sierra, L., P. Stoykova, and Z. L. Nikolov. 2018. "Extraction and Fractionation of Microalgae-Based Protein Products." *Algal Research* 36: 175–192. https://doi.org/10.1016/j.algal.2018.10.023.

Srimongkol, P., P. Songserm, K. Kuptawach, et al. 2023. "Sulfated Polysaccharides Derived From Marine Microalgae, Synechococcus sp. VDW, Inhibit the Human Colon Cancer Cell Line Caco-2 by Promoting Cell Apoptosis via the JNK and p38 MAPK Signaling Pathway." *Algal Research* 69: 102919. https://doi.org/10.1016/j.algal.2022.102919.

Stirk, W. A., P. Bálint, M. Vambe, et al. 2020. "Effect of Cell Disruption Methods on the Extraction of Bioactive Metabolites From Microalgal Biomass." *Journal of Biotechnology* 307: 35–43. https://doi.org/10.1016/j.jbiotec.2019.10.012.

Sun, Y., H. Chen, W. Chen, Q. Zhong, M. Zhang, and Y. Shen. 2022. "Effects of Ultrasound Combined With Preheating Treatment to Improve the Thermal Stability of Coconut Milk by Modifying the Physicochemical Properties of Coconut Protein." *Food* 11, no. 7: 1042. https://doi.org/10.3390/foods11071042.

Tang, C.-H., and X. Sun. 2011. "A Comparative Study of Physicochemical and Conformational Properties in Three Vicilins From Phaseolus Legumes: Implications for the Structure–Function Relationship." *Food Hydrocolloids* 25, no. 3: 315–324. https://doi.org/10.1016/j.foodhyd.2010.06.009.

Taragjini, E., M. Ciardi, E. Musari, et al. 2022. "Pilot-Scale Production of *A. platensis*: Protein Isolation Following an Ultrasound-Assisted Strategy and Assessment of Techno-Functional Properties." *Food and Bioprocess Technology* 15, no. 6: 1299–1310. https://doi.org/10.1007/s11947-022-02789-1.

Teuling, E., J. W. Schrama, H. Gruppen, and P. A. Wierenga. 2019. "Characterizing Emulsion Properties of Microalgal and Cyanobacterial Protein Isolates." *Algal Research* 39: 101471. https://doi.org/10.1016/j.algal.2019.101471.

Tian, R., J. Feng, G. Huang, et al. 2020. "Ultrasound Driven Conformational and Physicochemical Changes of Soy Protein Hydrolysates." *Ultrasonics Sonochemistry* 68: 105202. https://doi.org/10.1016/j.ultsonch.2020.105202.

Timilsena, Y. P., R. Adhikari, C. J. Barrow, and B. Adhikari. 2016. "Physicochemical and Functional Properties of Protein Isolate

Produced From Australian Chia Seeds." *Food Chemistry* 212: 648–656. https://doi.org/10.1016/j.foodchem.2016.06.017.

Uenojo, M., M. R. Maróstica Junior, and G. M. Pastore. 2007. "Carotenóides: Propriedades, aplicações e biotransformação para formação de compostos de aroma." *Química Nova* 30, no. 3: 616–622. https://doi.org/10.1590/S0100-40422007000300022.

Ursu, A.-V., A. Marcati, T. Sayd, V. Sante-Lhoutellier, G. Djelveh, and P. Michaud. 2014. "Extraction, Fractionation and Functional Properties of Proteins From the Microalgae *Chlorella vulgaris*." *Bioresource Technology* 157: 134–139. https://doi.org/10.1016/j.biortech.2014.01.071.

Vieira, B. B., J. Soares, M. L. Amorim, et al. 2021. "Optimized Extraction of Neutral Carbohydrates, Crude Lipids and Photosynthetic Pigments From the Wet Biomass of the Microalga *Scenedesmus obliquus* BR003." *Separation and Purification Technology* 269: 118711. https://doi.org/10.1016/j.seppur.2021.118711.

Waghmare, A. G., M. K. Salve, J. G. LeBlanc, and S. S. Arya. 2016. "Concentration and Characterization of Microalgae Proteins From *Chlorella pyrenoidosa*." *Bioresources and Bioprocessing* 3, no. 1: 16. https://doi.org/10.1186/s40643-016-0094-8.

Wang, L., X. Zhang, X. Wang, A. Hui, F. Xie, and X. Wu. 2025. "Comparative Analysis of Structural Characterisation and Gel Properties of Blended/Co-Precipitated Soy-Pea Dual-Protein." *Food* 14, no. 16: 2867. https://doi.org/10.3390/foods14162867.

Wang, X., X. Ni, C. Duan, et al. 2024. "The Effect of Ultrasound Treatment on the Structural and Functional Properties of *Tenebrio molitor* Myofibrillar Protein." *Food* 13, no. 17: 2817. https://doi.org/10.3390/foods13172817.

Wellburn, A. R. 1994. "The Spectral Determination of Chlorophylls A and B, as Well as Total Carotenoids, Using Various Solvents With Spectrophotometers of Different Resolution." *Journal of Plant Physiology* 144, no. 3: 307–313. https://doi.org/10.1016/S0176-1617(11)81192-2.

Wen, C., J. Zhang, H. Zhang, Y. Duan, and H. Ma. 2019. "Effects of Divergent Ultrasound Pretreatment on the Structure of Watermelon Seed Protein and the Antioxidant Activity of Its Hydrolysates." *Food Chemistry* 299: 125165. https://doi.org/10.1016/j.foodchem.2019.125165.

Yu, J., B. Ding, R. Li, et al. 2024. "The Efficient Capture of Polysaccharides in Tetradesmus Obliquus of Indole-3-Acetic Acid Coupling Sludge Extraction." *Science of the Total Environment* 912: 168963. https://doi.org/10.1016/j.scitotenv.2023.168963.

Zhao, F., X. Liu, X. Ding, H. Dong, and W. Wang. 2019. "Effects of High-Intensity Ultrasound Pretreatment on Structure, Properties, and Enzymolysis of Soy Protein Isolate." *Molecules* 24, no. 20: 3637. https://doi.org/10.3390/molecules24203637.